Geosci. Model Dev. Discuss., 7, 131–179, 2014
www.geosci-model-dev-discuss.net/7/131/2014/
doi:10.5194/gmdd-7-131-2014

Geoscientific Model Development Discussions
Open Access

Application of a global nonhydrostatic model with a stretched-grid system to regional aerosol simulations around Japan

D. Goto[1], T. Dai[2,3], M. Satoh[3,4], H. Tomita[4,5], J. Uchida[3], S. Misawa[3], T. Inoue[3], H. Tsuruta[3], K. Ueda[1], C. F. S. Ng[1], A. Takami[1], N. Sugimoto[1], A. Shimizu[1], T. Ohara[1], and T. Nakajima[3]

[1]National Institute for Environmental Studies, Tsukuba, Japan
[2]State Key Laboratory of Numerical Modeling for Atmospheric Sciences and Geophysical Fluid Dynamics, Institute of Atmospheric Physics, Chinese Academy of Sciences, Beijing, China
[3]Atmosphere and Ocean Research Institute, University of Tokyo, Kashiwa, Japan
[4]Japan Agency for Marine-Earth Science and Technology, Yokohama, Japan
[5]Advanced Institute for Computational Science, RIKEN, Kobe, Japan

Received: 15 November 2013 – Accepted: 20 December 2013 – Published: 8 January 2014

Correspondence to: D. Goto (goto.daisuke@nies.go.jp)

Published by Copernicus Publications on behalf of the European Geosciences Union.

Abstract

An aerosol-coupled global nonhydrostatic model with a stretched-grid system has been developed. Circulations over the global and target domains are simulated with a single model, which includes fine meshes covering the target region to calculate meso-scale circulations. The stretched global model involves relatively low computational costs to simulate atmospheric aerosols with fine horizontal resolutions compared with a global uniform nonhydrostatic model. As opposed to general regional models, neither a nesting technique nor boundary conditions are required. In this study, we developed a new air-quality model for the simulation of areas surrounding Tokyo, Japan, with a maximum horizontal resolution of approximately 10 km. We determined that this model was capable of simulating meteorological fields and anthropogenic primary particles, e.g., elemental carbon, and secondary particles, such as sulfate, with comparable results to those found with in-situ measurements and with other regional models. By combining the meteorological fields obtained from an atmosphere-ocean coupled model, we also applied the new model to a climate scenario experiment of $PM_{2.5}$ (aerosol particles with diameters less than 2.5 µm) over Japan with a high horizontal resolution to assess the public health impact at the prefecture scale.

1 Introduction

Aerosols can greatly affect regional air quality and contribute to global climate change (Forster et al., 2007). Recently, transboundary aerosol pollution, whereby regions beyond a given country's borders are affected by the aerosols generated in that country, has been of increasing concern (Ramanathan et al., 2008; Yu et al., 2012). The ongoing rapid economic growth in developing countries has the potential to exacerbate this issue (UNEP and WMO, 2011). Air pollution generated by aerosols is a critical public health issue due to the deleterious effects of these particles on human health (Dockery et al., 1993; Pope et al., 2009). Aerosols, which scatter and absorb solar

GMDD
7, 131–179, 2014

radiation and act as cloud condensation nuclei, can directly and indirectly change the Earth's radiation budget. The majority of aerosols are emitted from localized areas, which are referred to as hotspots, such as megacities and biomass-burning regions, and are spread throughout the world via atmospheric transport (e.g., Ramanathan et al., 2008). Therefore, global aerosol-transport models should consider the important regional-scale characteristics of aerosol hotspots to reliably estimate their impacts on air quality and climate change.

Most existing global aerosol-transport models do not address the spatial variability of aerosols in the vicinity of hotspots due to their coarse horizontal resolution of 100–300 km (Kinne et al., 2006; Textor et al., 2006). In addition, global aerosol-transport models with coarse resolutions frequently adopt a spectral transform method with a hydrostatic approximation to effectively calculate atmospheric dynamics. This spectral transform method is less effective than the grid-point method (Stuhne and Peltier, 1996; Taylor et al., 1997; Randall et al., 2000) for high horizontal resolutions (Tomita et al., 2008). Models that employ the grid-point method flexibly define grid points to enable an adaptive focus on study regions. Thus, global models based on the grid-point method seem most appropriate for use in simulating aerosol transport from hotspots to outflow regions.

For this purpose, we utilized the global Nonhydrostatic Icosahedral Atmospheric Model (NICAM) developed by Tomita and Satoh (2004) and Satoh et al. (2008). NICAM has been employed for the global simulation of atmospheric processes with high-resolution grid spacing, whose size is comparable to the typical deep convective cloud scale. Miura et al. (2007) performed a one-week computation with a horizontal resolution of 3.5 km using the Earth Simulator at the Japan Agency for Marine-Earth Science and Technology (JAMSTEC) to successfully simulate a Madden-Julian Oscillation (MJO) event. Suzuki et al. (2008) implemented an aerosol transport model named the Spectral Radiation-Transport Model for Aerosol Species (SPRINTARS; Takemura et al., 2005) in NICAM (we refer to this aerosol-coupled model as NICAM-SPRINTARS) and performed a one-week simulation with a horizontal resolution of 7 km using the Earth

GMDD
7, 131–179, 2014

Simulator. Although these global, highly resolved calculations are promising with regard to long-term climate simulations, their requirement of vast computer resources substantially limits their use in short-duration and/or case-specific simulations due to the current limitations of computational resources. To overcome this limitation, we adopt a compromise approach based on a new grid transformation named the stretched grid system, which was developed and implemented in NICAM by Tomita (2008a) for computationally effective simulations in the target region (see, also, Satoh et al., 2010). We applied this approach to NICAM-SPRINTARS, which we named Stretch-NICAM-SPRINTARS, to calculate aerosol transport processes with high horizontal resolutions over aerosol source regions.

In this study, we focused on the Kanto region surrounding Tokyo, which is one of the largest megacities in the world and is located in eastern Japan (Fig. 1). More than 30 million people in this region are potentially vulnerable to air pollution. Within the Kanto region, intensive measurements (Fine Aerosol Measurement and Modeling in Kanto Area, FAMIKA) were performed during summer 2007 to monitor the air quality, including aerosol chemical compounds (Hasegawa et al., 2008; Fushimi et al., 2011). We simulated aerosol spatial distributions during this period using Stretch-NICAM-SPRINTARS with a horizontal resolution of approximately 10 km over the Kanto region. Because the model framework of Stretch-NICAM-SPRINTARS is identical to that of globally uniformed grid simulation, with the exception of the grid configuration, and involves lower computational costs than global simulations, the investigation of the model performance of Stretch-NICAM-SPRINTARS can be simply and effectively extended to improve the original NICAM-SPRINTARS with globally uniform high resolution for near-future simulations.

Stretch-NICAM-SPRINTARS is a new type of model that is also applicable for predicting the spatial distribution of aerosols under various future scenarios with a higher horizontal resolution than demonstrated in previous studies, such as Koch et al. (2007) and Carmichael et al. (2009). Stretch-NICAM-SPRINTARS does not require a nesting technique or boundary conditions, unlike general regional models. As a result, the simulations of transboundary air pollution, which is expected to increase in Asia (Takemura, 2012), are potentially superior to those obtained by general regional models. Given the heterogeneous distribution of populations in terms of the geography of megacities, Stretch-NICAM-SPRINTARS enables improved estimates of aerosol impacts on human health for future scenarios on a local scale, for example, within prefectures or municipalities of a country. Populations in megacities, particularly those in Asia, are highly susceptible to air pollution (UNEP and WMO, 2011). To predict the extent to which ambient particulates will affect the population in 2030, we performed a scenario experiment involving $PM_{2.5}$ (aerosol particles with diameters less than 2.5 µm) around Japan by forcing Stretch-NICAM-SPRINTARS with meteorological fields obtained by an atmosphere-ocean coupled general circulation model (AOGCM), which is referred to as the Model for Interdisciplinary Research on Climate (MIROC) and was developed by the Atmosphere and Ocean Research Institute at the University of Tokyo (AORI/UT), the National Institute for Environmental Studies (NIES) and JAMSTEC (Watanabe et al., 2010). Based on the results of this experiment, we estimated human mortality impacts attributable to $PM_{2.5}$ exposure under the future scenario of Representative Concentration Pathway (RCP) 4.5 in 2030 and accounting for excess mortality, population distributions, and ambient $PM_{2.5}$ changes in a given area.

This paper is organized as follows: Stretch-NICAM-SPRINTARS and the experimental design are described in Sect. 2. In Sect. 3, the model results are validated using in-situ measurements in terms of meteorological fields and aerosol species, especially elemental carbon (EC), sulfate and SO_2. In Sect. 4, we present the validation of total aerosol amounts, i.e., $PM_{2.5}$, and an application of the proposed Stretch-NICAM-SPRINTARS using the results of the future scenario experiment by "MIROC-AOGCM" for the estimation of health impacts. The conclusions are summarized in Sect. 5.

GMDD
7, 131–179, 2014

D. Goto et al.

2 Model description

2.1 Nonhydrostatic Icosahedral Atmospheric Model (NICAM)

NICAM, which employs an icosahedral grid-point method with a nonhydrostatic equation system (Tomita and Satoh, 2004; Satoh et al., 2008), is run with a maximum horizontal resolution of 3.5 km (Tomita et al., 2005; Miura et al., 2007) and can be applied to a transport model of aerosols and gases as a conventional atmospheric general circulation model (Suzuki et al., 2008; Niwa et al., 2011; Dai et al., 2014). NICAM can also be employed for regional-scale simulations by adopting a stretched-grid system (Tomita, 2008a; Satoh et al., 2010). The stretched icosahedral grid was developed from a general grid transformation method, i.e., the Schmidt transformation method, for a horizontal grid system on a sphere. In the Schmidt transformation, the grid interval on a sphere lacks uniformity with a finer horizontal resolution close to the center of the target region. Tomita (2008a) showed that the Schmidt transformation minimizes potential errors involving the isotropy and homogeneity of the target region. The stretched-grid system can solve the main problems associated with commonly used regional models, which occur from artificial perturbations near boundary areas in cases where meteorological and aerosol fields are prescribed. In addition, the computational cost of the stretched-grid system is substantially lower than that of a global calculation under the same horizontal resolution in the target region. For example, when the globally uniform grid with a maximum horizontal resolution of 10 km is applied to the global simulation, the minimum required theoretical computational cost is 256 times higher than the cost of the stretched-grid system in this study. The model framework of the stretched global model is identical to that of the uniformed global model without special modifications. These advantages can facilitate additional developments by testing a new scheme with minimal computational cost. Compared with general regional models, the stretched-grid system is more suitable for the current study, which aimed to extend its use to the global uniform high-resolution NICAM-SPRINTARS.

GMDD
7, 131–179, 2014

In this study, we adopt the stretched-grid system to focus on the Kanto region, including Tokyo, using glevel-6 resolution, in which “glevel” is the number of divisions of an icosahedron used to construct the horizontal grid, and the stretched ratio of 100, which is the ratio of the largest horizontal grid spacing located on the opposite side of the earth from Tokyo to the smallest horizontal grid spacing near Tokyo. As a result, a minimum horizontal resolution of 11 km around the center (140.00° E, 35.00° N) was used. NICAM implements comprehensive physical processes of radiation, boundary layer and cloud microphysics. The radiation transfer model is implemented in NICAM with the k-distribution radiation scheme MSTRN, which incorporates scattering, absorption and emissivity by aerosol and cloud particles as well as absorption by gaseous compounds (Nakajima et al., 2000; Sekiguchi and Nakajima, 2008). The vertical turbulent scheme comprises the level 2 scheme of turbulence closure by Mellor and Yamada (1974), Nakanishi and Niino (2004, 2009) and Noda et al. (2009). The cloud microphysics consist of the six-class one-moment bulk scheme (water vapor, cloud water, rain, cloud ice, snowflakes and graupel) (Tomita, 2008b). Based on our experience in previous studies, we did not employ cumulus parameterization in this study (e.g., Tomita et al., 2005; Sato et al., 2009; Nasuno, 2013). The vertical resolutions were set to the 40 layers of z-levels, and the timestep was set to 20 s.

2.2 SPRINTARS

Based on the approach of Suzuki et al. (2008), the three-dimensional aerosol-transport model – Spectral Radiation-Transport Model for Aerosol Species (SPRINTARS; Takemura et al., 2000, 2002, 2005; Goto et al., 2011a, b, c) – was coupled to NICAM in this study. The SPRINTARS model calculates the mass mixing ratios of the primary tropospheric aerosols, i.e., carbonaceous aerosol (EC and OC, organic carbon), sulfate, soil dust, sea salt and the precursor gases of sulfate, namely, SO_2 and dimethylsulfide. The aerosol module considers various processes, such as emission, advection, diffusion, sulfur chemistry, wet deposition and dry deposition, including gravitational settling. For carbonaceous aerosols, the 50 % mass of EC from fossil

GMDD
7, 131–179, 2014

fuel sources is composed of externally mixed particles, whereas other carbonaceous particles are emitted and treated as internal mixtures of EC and OC (EC-OC internal mixture). Biogenic secondary organic aerosols (SOAs) from monoterpenes are treated but are greatly simplified. In addition, anthropogenic SOAs from toluene and xylene are disregarded in this study. The particle size distribution of these particles are assumed to be a logarithmic normal size distribution using a 1-modal approach with dry mode radii of 18, 100, 80 and 69.5 nm, for pure EC, EC-OC internal mixture, biogenic SOA and externally mixed sulfate, respectively (Goto et al., 2011a). The hygroscopicities, densities and refractive indices for the aerosols are set to the same values used by Takemura et al. (2002) and Goto et al. (2011a). The combinations of the pre-calculated cross-sections of the extinction and simulated mixing ratios for each aerosol species provide the simulated aerosol extinction coefficient for each timestep of the model (Takemura et al., 2002). The atmospheric removal of aerosols in SPRINTARS includes wet (due to rainout and washout) and dry (due to turbulence and gravity) deposition processes. In this study, the particle mass concentrations for diameters less than 2.5 µm (defined as $PM_{2.5}$) are calculated by summing all carbonaceous, sulfate and ammonium aerosols. Because this model cannot directly predict ammonium compounds, we assumed their concentration as the multiplication of the mass concentration of sulfate by 0.27, which is the molar ratio of ammonium ion to ammonium sulfate. The nitrate concentrations in this study, with the target of summer in Japan, can be disregarded.

2.3 Design of the standard experiment

The target period comprises one month in August 2007, in which an intensive measurement of aerosol chemical species was conducted under Project FAMIKA (Hasegawa et al., 2008; Fushimi et al., 2011). The six-hour meteorological fields (wind and temperature) were nudged above a height of 2 km using NCEP-FNL reanalysis data (http://rda.ucar.edu/datasets/ds083.2/). The one-hour sea surface temperature was also nudged using the NCEP-FNL data. The initial conditions were prescribed by the

NCEP-FNL data for the meteorological fields and the spinup results of the Stretch-NICAM-SPRINTARS model for the aerosol fields, respectively.

The emission inventories of anthropogenic EC, OC and SO_2 in this experiment were prepared by EAGrid2000 with a horizontal resolution of 1 km over Japan (Kannari et al., 2007), REAS version 2 with a horizontal resolution of 0.25° over Asia (Kurokawa et al., 2013) and the AeroCom inventory with a horizontal resolution of 1° over other areas of the world (Diehl et al., 2012). Because EAGrid2000 does not explicitly estimate EC and OC inventories, we estimated the inventories to be consistent with those from previous studies (Morino et al., 2010a, b; Chatani et al., 2011) by modifying the $PM_{2.5}$ inventory of EAGrid2000 using scaling factors of EC/$PM_{2.5}$ and OC/$PM_{2.5}$ based on sources. These inventories of anthropogenic EC and SO_2 in 2007 are described in Figs. 2a and 3a. The emissions of SO_2 from volcanoes in Japan, such as Miyakejima and Sakura-jima, were obtained from statistical reports (http://www.seisvol.kishou.go.jp/tokyo/volcano.html) by the Japan Meteorological Agency (JMA). To calculate the sulfur chemistry in SPRINTARS, the distributions of three hourly averaged monthly oxidants (hydroxyl radicals, ozone and hydrogen peroxide) were derived from a global chemical transport model coupled to MIROC, named MIROC-CHASER (Sudo et al., 2002).

In this study, we focused on the aerosol chemical component of EC as the primary particle and sulfate as the secondary particle. To evaluate the model results over the Kanto region, we used observations of the surface mass concentrations of EC and sulfate in four cities under Project FAMIKA: Maebashi/Gunma (139.10° E, 36.40° N), Kisai/Saitama (139.56° E, 36.09° N), Komae/Tokyo (139.58° E, 35.64° N) and Tsukuba/Ibaraki (140.12° E, 36.05° N). The EC particles in $PM_{2.5}$ were collected every six hours with quartz fiber filters and analyzed with the thermal/optical method according to the IMPROVE protocol (Chow et al., 2001). The sulfate particles in $PM_{2.5}$ were also collected every six hours with Teflon filters and analyzed by ion chromatography. In addition to the limited FAMIKA dataset, we also utilized measurements taken by the EANET (Acid Deposition Monitoring Network in East Asia;

GMDD
7, 131–179, 2014

http://www.eanet.asia/index.html) to assess the monthly mean concentrations of sulfate and SO_2 at ten sites throughout Japan. To validate the concentration of SO_2 for the Kanto region, we accessed monitoring stations operated by Japanese and local governments.

In the validation of the meteorological fields simulated by Stretch-NICAM-SPRINTARS, we obtained measurements for the meteorological parameters (temperature, relative humidity (RH) and wind) at or near the sites of Project FAMIKA and other cities in the Kanto region: Tsuchiura/Ibaraki (140.20° E, 36.07° N), which is the city nearest to Tsukuba; Yokohama/Kanagawa (139.64° E, 35.45° N); Chiba/Chiba (140.12° E, 35.62° N); Adachi/Tokyo (139.82° E, 35.77° N); and Machida/Tokyo (139.43° E, 35.53° N), which is the city nearest to Komae, as shown in Fig. 1b. For precipitation, we used a measurement taken by the Automated Meteorological Data Acquisition System (AMeDAS) at Yokohama; Chiba; Tsukuba; Tokyo, which is near Adachi; Maebashi; Huchu, which is near Machida; and Konosu, which is near Kisai. To evaluate the spatial patterns of the precipitation obtained by Stretch-NICAM-SPRINTARS, we used the quantities of the monthly mean precipitation around Japan that were derived from the Global Satellite Mapping of Precipitation (GSMaP; Okamoto et al., 2005; Kubota et al., 2007; Aonashi et al., 2009; Ushio et al., 2009) and the forecast Grid Point Value (GPV) processed by the JMA.

To evaluate the quantities of the total aerosol amounts, such as $PM_{2.5}$, we compared the simulated $PM_{2.5}$ concentrations with the observations at the FAMIKA sites and other monitoring stations operated by the Japanese and local governments of Kawasaki/Kanagawa, which is the city nearest to Yokohama; Machida/Tokyo; Koutou/Tokyo, which is site nearest to the site of Adachi/Tokyo; Osaka/Osaka (135.53° E, 34.68° N); Amagasaki/Hyogo (135.42° E, 34.72° N); and Nonodake/Miyagi (141.17° E, 38.55° N). The $PM_{2.5}$ concentrations were continuously observed using tapered element oscillating microbalance (TEOM).

In Tsukuba and Chiba, light detection and ranging (LIDAR) measurements operated by the NIES of Japan were also available (Sugimoto et al., 2003; Shimizu et al., 2004).

GMDD
7, 131–179, 2014

D. Goto et al.

The LIDAR unit measured vertical profiles of the backscattering intensity at 532 and 1064 nm and the depolarization ratio at 532 nm. The backscattering intensity was converted to the extinction coefficient, and the depolarization ratio distinguished the extinction between spherical and non-spherical particles. In this study, we only used vertical profiles of the extinction for spherical particles. A detailed algorithm was provided by Sugimoto et al. (2003) and Shimizu et al. (2004).

2.4 Scenario experiment

In previous future-scenario experiments, general climate models such as MIROC-AOGCM (Watanabe et al., 2010) were incapable of estimating the impacts of $PM_{2.5}$ on human health within the prefectures of Japan due to their coarse grid sizes. In addition, the model used in the current study, Stretch-NICAM-SPRINTARS, cannot be used for a long-term simulation. Therefore, we combined Stretch-NICAM-SPRINTARS with MIROC-AOGCM by nudging the meteorological results of MIROC-AOGCM under the scenario experiment of Representative Concentration Pathway (RCP) 4.5 in August 2030. In this study, we selected target results of temperature and precipitation fluxes in the representative years within ten years of 2026–2035.

The emission inventories of anthropogenic EC, OC and SO_2 from anthropogenic sources in the scenario experiment were based on the IPCC inventory, including RCP4.5 with a global horizontal resolution of 0.5° (Lamarque et al., 2010; Moss et al., 2010). However, due to the coarse grid size of the emission inventory around Japan, we multiplied the inventory of EAGrid2000 (Kannari et al., 2007) by scaling factors, which were estimated from the results of IPCC emission inventories for each compound. For the emission inventory, to eliminate an outlier during year 2026–2035 used in the present study, we averaged results from the ten years. Monthly mean oxidant distributions for sulfate formation were also obtained from the MIROC-CHASER model (Sudo et al., 2002) used in the MIROC-AOGCM scenario experiments in the same period. Inventories of the biomass burning over forest fires outside Japan were disregarded in the scenario experiment because a minimal impact on the aerosol distribution around

Japan during the summer is expected. Figures 2b and 3b also illustrate the emission inventories of EC and SO_2 in 2030 under the RCP4.5 scenario experiment. The quantities of EC and SO_2 emissions in Japan exhibit a decreasing trend from the present to 2030, whereas the quantities of EC and SO_2 emissions in China and Korea exhibit an increasing trend.

To quantify the health impact of exposure to ambient $PM_{2.5}$, we estimated the excess mortality per grid attributable to $PM_{2.5}$, which is denoted by $D(x)$, using the following function:

$$D(x) = N(x)\{\exp(\beta) - 1\}\{P(x) - P_0\}, \quad (1)$$

where β is the linear slope between $PM_{2.5}$ and mortality. A similar association was previously employed for the estimation of the excess mortality due to high temperature (Chung et al., 2009). The β value for Japan is set to 0.53 % per 10 $\mu g\, m^{-3}$ increase in $PM_{2.5}$ (Ueda et al., 2009). The P value is set to 15 $\mu g\, m^{-3}$ based on the environmental quality standards for atmospheric $PM_{2.5}$ in Japan because the threshold value cannot be directly derived from the observed dataset. $P(x)$ is the $PM_{2.5}$ mass concentration in units of $\mu g\, m^{-3}$ obtained from Stretch-NICAM-SPRINTARS in one NICAM grid, including the position x, and $N(x)$ is the population above 64 yr of age who are at risk due to exposure to air pollutants per grid x (Ueda et al., 2009). The population distributions were represented by grids with dimensions of 1 km by 1 km. The grid containing the position x and the excess mortality were estimated in the same horizontal resolution as the population distribution.

3 Validation of Stretch-NICAM-SPRINTARS

3.1 Meteorological fields

To evaluate the model performances of the meteorological fields obtained by Stretch-NICAM-SPRINTARS, we used the observed temperature, RH, wind and precipitation at each station over the Kanto region shown in Fig. 1b. The results and summary are shown in Figs. 4 to 7 and Table 1. Figure 4 illustrates the temporal variations of temperature at a height of 2 m. The temporal variations in the simulated temperature are generally comparable to those in the observed temperatures with root-mean-square-error (RMSE) values of less than 3 °C, with the exception of the results obtained for Maebashi and Machida. At these two sites, the mean values of the simulated temperatures are lower than those of the observed temperatures by a maximum of 3 °C. The correlation coefficients (R) between the simulations and observations range from 0.7–0.8, as shown in Table 1. Figure 5 shows the temporal variations in RH at a height of 2 m. The monthly average temporal variations in the simulated RH are similar to the observations, with the RMSEs in the range of 10–15 %. The R values of RH between the simulation and observations are approximately 0.6–0.8, as shown in Table 1.

The temporal variation in the wind direction and speed simulated by Stretch-NICAM-SPRINTARS are compared with the observations in Figs. 6 and 7. Near the southern part of the Kanto region (Yokohama, Tsuchiura, Adachi and Machida), with the exception of Chiba, the simulated wind directions are generally comparable to the observations, with a slight overestimation of the simulated wind speed compared with the observations. At these four sites, the R values and RMSE values range from approximately 0.5–0.6 and from approximately 1.5–2.2 $m\,s^{-1}$, respectively. In Chiba located near the ocean, the R value of wind speed between the simulation and observations is 0.27, whereas the simulated wind directions generally agree with the observations. Conversely, at Maebashi and Kisai, the daily variations in the simulated wind direction differ significantly from those in the observations, in which the southern winds and northern winds frequently occur during the day and night, respectively, for example, during 5–12 August. The R values for wind speed between the simulation and observations at these sites are estimated to be approximately 0.3–0.4. The results of the meteorological fields at Maebashi and Kisai, which are surrounded by or are located relatively close to high mountains, indicate that the horizontal resolution of 10 km in this study using Stretch-NICAM-SPRINTARS could not completely resolve the topography.

As a result, it may be inadequate to simulate the wind patterns and diurnal transitions near high mountains.

Figure 8 shows the temporal variations in the amount of precipitation per day at each site. During August 2007 in the Kanto region, the observed precipitation is extremely limited and sometimes localized. The temporal variations in the simulated precipitation are generally similar to those in the observations. However, the precipitation modeled by Stretch-NICAM-SPRINTARS on 19 and 23 August is higher than the observations by more than 30 $mm\,day^{-1}$. Stretch-NICAM-SPRINTARS does not always capture a sudden shower, as general meteorological models cannot properly simulate this type of precipitation system. This overestimation may have an impact on the monthly mean precipitation shown in Fig. 9, which compares the Stretch-NICAM-SPRINTARS simulated precipitation with the GPV- and GSMaP-derived results. The overestimation of the precipitation obtained by Stretch-NICAM-SPRINTARS compared with the observations is also seen in the Sea of Japan, Kyusyu, and the main island of Japan. All results generally show similar patterns of the occurrence of heavy precipitation in the East China Sea and the Sea of Japan near the Japan coast, especially near Okinawa, the southern part of South Korea and North Korea. Therefore, Stretch-NICAM-SPRINTARS can generally simulate the meteorological fields in the present target regions.

3.2 Aerosol fields

3.2.1 Evaluation using measurements

Figure 10 illustrates the temporal variations in the surface EC mass concentration obtained by Project FAMIKA at the four stations (Maebashi, Kisai, Komae and Tsukuba). The temporal variation and the average correspond with the observations obtained for Komae, as shown in Fig. 10c. For Tsukuba, which is shown in Fig. 10d, the simulated EC concentrations tend to be underestimated compared with the observed concentrations, especially during the daytime. However, in some instances, these results are comparable with the observations. Conversely, the temporal variation in the simulated

GMDD
7, 131–179, 2014

EC concentrations and the average EC concentrations at Maebashi and Kisai are underestimated compared with the observations by a factor of three to five. At the same sites, simulated sulfur components (sulfate and SO_2) are compared with the observations in Figs. 11 and 12. The observed SO_2 represents the ensemble results of monitoring stations operated by Japanese and local governments around each FAMIKA site. The averaged differences between the simulated and observed sulfate mass concentrations are within approximately 10 % at Maebashi and Tsukuba, −40 % at Komae and +50 % at Kisai. At all sites, the temporal variations of the simulated sulfate are generally comparable to those of the observations, whereas differences in the sulfate between the simulation and observations are somewhat greater on 7 August in Maebashi and on 6 August in Kisai, Komae and Tsukuba. However, differences between the simulated and observed SO_2 concentrations at all sites are within approximately 30 %. The temporal variations in the simulated SO_2 concur with those in the observations. To assess the performance of Stretch-NICAM-SPRINTARS in simulating the aerosol distribution over Japan, we compared the August averages of the simulated sulfate and SO_2 with the available measurements of EANET (Fig. 13). The results indicate that the simulated sulfate concentrations tend to be underestimated by approximately 40 % compared with the observed sulfate concentrations. However, the correlation between the simulation and observation is adequately acceptable ($R = 0.79$ or $R = 0.86$, with the exception of Hedo). At Hedo located in the southwestern islands of Japan, the overestimation of the simulated precipitation shown in Fig. 9 may cause the underestimation of the simulated sulfate concentrations. The simulated and observed SO_2 concentrations also correlate, with an R value of 0.95. Figure 14 shows the monthly averaged sulfate and SO_2 in August 2007. The SO_2, which is a primary product, is localized near the source areas, whereas sulfate, which is as a secondary product, is distributed from the source to the outflow areas. In the Kanto region, for example, sulfate from transboundary and domestic pollution is effectively simulated by Stretch-NICAM-SPRINTARS.

GMDD
7, 131–179, 2014

3.2.2 Uncertainty in the simulation

Sensitivity tests were conducted to examine potential uncertainties derived from prescribed datasets related to EC and sulfate for the Stretch-NICAM-SPRINTARS simulations. For the EC sensitivity tests, the emission quantities were set to half and twice of those used in the standard run in this study. The results for the FAMIKA sites are shown in Fig. 15a in which the bars indicate the simulated EC concentrations for both sensitivity tests. For the majority of the sites, with the exception of Komae, the results obtained by the sensitivity experiments remain underestimated compared with the measurements. The underestimation of the EC mass concentrations at Maebashi and Kisai was also shown by the previous studies of Morino et al. (2010a, b) and Shimadera et al. (2013), who calculated EC concentrations using the Community Multiscale Air Quality (CMAQ) driven by the Weather Research and Forecasting (WRF) model named WRF-CMAQ with a horizontal resolution of 5 km. WRF-CMAQ employs an emission inventory that is similar to that in the present study. The difference in the EC concentrations at Maebashi between the present study and the previous studies using WRF-CMAQ is partly caused by the difference in the horizontal resolution, which is most likely critical for properly simulating the air pollution delivered by the meteorological wind fields from the center of the Kanto region. However, Fushimi et al. (2011) and Chatani et al. (2014) suggested that the difference in the EC concentrations between WRF-CMAQ and the measurements is largely attributed to an underestimation of the EC emission inventory, especially open biomass burning from domestic sources. Therefore, the same factor may be applicable to the present results using Stretch-NICAM-SPRINTARS.

Sensitivity experiments of the SO_2 emissions and the prescribed hydroxyl radical used in sulfur chemistry were executed under half and twice the amounts used in the standard experiment. Figure 15b shows that the sensitivity of the hydroxyl radical concentrations to the simulated sulfate concentration is substantially smaller than that to the SO_2 emissions. Compared with the SO_2 emissions used in the standard

GMDD
7, 131–179, 2014

experiment, the doubled amount of SO_2 emissions can overcome the slight underestimation of the simulated sulfate compared with the observations. We also determined that the sensitivities of the other oxidants to the simulated sulfate concentrations were minimal (not shown). These results from the sensitivity experiments indicate that the offline prescribed oxidant used in this study is not as critical to the proper prediction of the sulfate concentrations over the Kanto region as the uncertainty in the quantity of SO_2 emissions. Therefore, we conclude that the simulations of Stretch-NICAM-SPRINTARS are generally successful in simulating the air pollution over Japan and are adequate as a new regional model for simulations over the Kanto region.

4 Application of Stretch-NICAM-SPRINTARS

4.1 $PM_{2.5}$

Figure 16 shows the temporal variation in the surface $PM_{2.5}$ mass concentration at the 11 sites over the Kanto region and in western and northern Japan. At all sites, the temporal variations in the simulated $PM_{2.5}$ are generally similar to those in the observed values; however, the simulated $PM_{2.5}$ concentrations are underestimated compared with the observations by a factor of two or three at the majority of sites and by approximately a factor of four at Maebashi. In addition to the issue of the poor model performance of the meteorological fields at Maebashi, the underestimation of secondary OC may be a critical issue, as suggested by previous studies (Matsui et al., 2009; Morino et al., 2010c). According to previous studies that employed regional aerosol-transport models (Morino et al., 2010b; Chatani et al., 2011), the underestimation of $PM_{2.5}$ is common because the measured concentrations of $PM_{2.5}$ include undefined chemical species with mean fractions ranging from approximately 30–50 % in the total $PM_{2.5}$ in the summer (datasets from the Tokyo Environment Agency and the Kawasaki Municipal Research Institute for Environmental Protection). Therefore, the undefined

GMDD
7, 131–179, 2014

chemical compounds in this study may account for a large portion of the difference between the simulated and the observed values.

To evaluate the vertical profiles of the $PM_{2.5}$ mass concentrations, we used the LIDAR observation operated by the NIES-Japan network. Figure 17 shows the average results for the simulated and observed extinction coefficient of the spherical particles at Chiba and Tsukuba in August. At both sites, the vertical profiles and the magnitudes below 3 km height of the simulated extinction values are comparable to the observed results, whereas the simulated extinction values tend to be smaller than the observed extinction values near the surface. These results are partly consistent with those obtained by the surface $PM_{2.5}$ comparison shown in Fig. 16. Therefore, when the results of $PM_{2.5}$ obtained by Stretch-NICAM-SPRINTARS are used in an estimation of health impacts due to $PM_{2.5}$, the bias should be minimized.

4.2 Scenario experiment and its health impact

Figure 18 illustrates the average simulated sulfate distribution by Stretch-NICAM-SPRINTARS near the surface around Japan in August 2030 for the RCP4.5 scenario experiment. As shown in Figs. 2 and 3, the domestic sources are expected to decrease from the present (2007) to 2030, whereas foreign sources will remain high under the scenario experiment of RCP4.5 in 2030. As a result, sulfate mass concentrations over the Kanto region decrease from the present to 2030. Conversely, sulfate over western Japan, especially Kyushu, where transboundary sources primarily contribute to the air quality, are expected to increase over the same period of time. Figure 19 shows the simulated sulfate mass concentrations obtained by Stretch-NICAM-SPRINTARS and MIROC-AOGCM in each prefecture over the Kanto region. The results for the MIROC-AOGCM indicate that the largest sulfate mass concentrations among the Kanto region occur in Ibaraki, which is unrealistic due to the coarse grid size, whereas the results for Stretch-NICAM-SPRINTARS calculated the largest sulfate mass concentrations in Kanagawa and Tokyo. In Tokyo, the difference between the mean concentration of sulfate estimated by Stretch-NICAM-SPRINTARS and that estimated by MIROC-AOGCM

GMDD
7, 131–179, 2014

is estimated to be approximately 2 $\mu g\,m^{-3}$. Given the large population in Tokyo in the Kanto region, such difference in $PM_{2.5}$ estimation can have huge implication on human health.

To estimate the health impact associated with $PM_{2.5}$, we assumed the $PM_{2.5}$ used in Eq. (1) is twice the value obtained via validations of Stretch-NICAM-SPRINTARS according to the results in the previous section. Figure 20 shows a preliminary example of the number of deaths caused by exposure to ambient $PM_{2.5}$ in each grid of 1 km by 1 km under the scenario experiment of RCP4.5 in 2030 using results obtained by Stretch-NICAM-SPRINTARS. The spatial distribution of the number of predicted deaths closely reflects population density. Although the concentrations of $PM_{2.5}$ concentrations in 2030 are lower than the current concentrations of $PM_{2.5}$, as suggested in Figs. 14 and 18, the highest number of deaths is caused by $PM_{2.5}$ in 2030, which is likely due to the higher susceptibility of the elderly population which is growing rapidly. Although the future concentrations of $PM_{2.5}$ are expected to decrease, the quantification of risk related to the future health impacts of $PM_{2.5}$ is crucial due to the aging society.

5 Summary

An aerosol-coupled global nonhydrostatic model, which is based on the aerosol module of Spectral Radiation-Transport Model for Aerosol Species (SPRINTARS) and the global cloud-resolving model of Nonhydrostatic Icosahedral Atmospheric Model (NICAM), with a horizontal resolution of approximately 10 km or less in the target region, is proposed in the present study. Circulations over both the global and target domains are solved with a single model, whose mesh size varies with fine meshes covering the target region, to calculate meso-scale circulations in the study region. The stretched global model requires relatively smaller computational costs to simulate atmospheric aerosols with fine horizontal resolutions compared with the global uniform nonhydrostatic model. As opposed to the general regional models, neither nesting techniques nor boundary conditions are required.

GMDD
7, 131–179, 2014

In this study, we developed the new air-quality model with a horizontal resolution of approximately 10 km to simulate aerosols in the megacities of the Kanto region of Japan, including Tokyo. We discovered that this model can simulate meteorological fields and anthropogenic primary particles, e.g., elemental carbon (EC), and secondary particles, e.g., sulfate, against in-situ measurements and other regional models. Therefore, this new seamless aerosol-transport model, which covers global to regional scales, can be applied to regional simulations. To effectively simulate areas around Japan, we have to address the following objectives: (1) to increase the horizontal resolution (less than 10 km) to properly resolve wind fields, which can greatly influence the delivery of air pollution from Tokyo to subcities such as Maebashi; (2) to accurately reproduce the precipitation caused by thermal lows, for example, by applying different schemes of cloud microphysics such as the double-moment bulk method proposed by Seiki and Nakajima (2013); (3) to use better emission inventories by developing a technique such as the Kalman smoother proposed by Schutgens et al. (2012); and (4) to implement a secondary organic aerosol (SOA) formed from both anthropogenic and biogenic sources in this model to simulate strong peaks of $PM_{2.5}$ in the daytime in the Kanto region. These issues may be directly connected to the further development of NICAM-SPRINTARS in both regional and global simulations.

We also succeeded in applying the stretched model to a climate scenario experiment involving $PM_{2.5}$ (aerosol particles with diameters less than 2.5 µm) over Japan with high horizontal resolution by including meteorological fields obtained from the atmosphere-ocean coupled model MIROC-AOGCM. The scenario experiment illustrated in this study at regional scales of 10 km grids has not been previously performed. The high horizontal resolution can provide estimates of human health impacts due to $PM_{2.5}$. The findings from our scenario experiment demonstrated the relevance of estimating future concentrations, particularly in aging populations with growing vulnerability. The novel technique that combines the use of Stretch-NICAM-SPRINTARS and pre-calculated climate simulations by MIROC-AOGCM can provide new opportunities to address the issue of regional air quality and its health impacts in densely populated megacities.

Acknowledgements. We acknowledge the developers of NICAM and SPRINTARS, especially K. Suzuki and T. Takemura, and the researchers from FAMIKA, especially S. Hasegawa and Y. Morino, and the researchers at AORI, especially Y. R. Li and A. Miyaji, for their assistance with processing the datasets. We are grateful to the local government measurements provided by the Tokyo Environment Agency, the Gunma Prefectural Institute of Public Health and Environmental Sciences and the Kawasaki Municipal Research Institute for Environmental Protection. We are also grateful to the working group members of Project SALSA, who were responsible for the scenario experiments, and the Ministry of Education, Culture, Sports and Science and Technology (MEXT)/Kakushin project, especially M. Watanabe, T. Nozawa and H. Kanai, for providing the MIROC datasets of climate simulation and emission inventories. Some of the authors were supported by Project SALSA, which is part of the Research Program on Climate Change Adaptation (RECCA) by the MEXT in Japan, the Global Environment Research Fund A-1101 of the Ministry of the Environment (MOE) in Japan, MOE/GOSAT, JST/CREST/EMS/TEEDDA, JAXA/EarthCARE, GCOM-C, MEXT/VL for climate diagnostics and MEXT/KAKENHI/Innovative Areas 2409. The model simulations were performed using supercomputer resources, SR16000 and PRIMEHPC FX10 from the University of Tokyo, Japan.

References

Aonashi, K., Awaka, J., Hirose, M., Kozu, T., Kubota, T., Liu, G., Shige, S., Kida, S. Seto, S., Takahashi, N., and Takayabu, Y. N.: GSMaP passive, microwave precipitation retrieval algorithm: Algorithm description and validation, J. Meteorol. Soc. Jpn., 87, 119–136, 2009.

Carmichael, G. R., Adhikari, B., Kulkarni, S., D'Allura, A., Tang, Y., Streets, D., Zhang, Q., Bond, T. C., Ramanathan, V., Jamroensan, A., and Marrapu, P.: Asian aerosols: current and year 2030 distributions and implications to human health and regional climate change, Environ. Sci. Technol., 43, 5811–5817, doi:10.1021/es8036803, 2009.

Chatani, S., Morikawa, T., Nakatsuka, S., and Matsunaga, S.: Sensitivity analysis of domestic emission sources and transboundary transport on $PM_{2.5}$ concentrations in three major Japanese urban areas for the year 2005 with the three-dimensional aie quality simulation, J. Jpn. Soc. Atmos. Environ., 46, 101–110, 2011 (in Japanese).

Chatani, S., Morino, Y., Shimadera, H., Hayami, H., Mori, Y., Sasaki, K., Kajino, M., Yokoi, T., Morikawa, T., and Ohara, T.: Multi-model analyses of dominant factors influencing elemental carbon in Tokyo metropolitan area of Japan, Aerosol Air Qual. Res., in press, 2014.

Chow, J. C., Watson, J. G., Crow, D., Lowenthal, D. H., and Merrifield, T.: Comparison of IMPROVE and NIOSH carbon measurements, Aerosol Sci. Tech., 34, 23–34, 2001.

Chung, J. Y., Honda, Y., Hong, Y.-C., Pan, X.-C., Guo, Y.-L., and Kim, H.: Ambient temperature and mortality: an international study in four capital cities of East Asia, Sci. Total Environ., 408, 390–396, doi:10.1016/j.scitotenv.2009.09.009, 2009.

Dai, T., Goto, D., Schutgens, N. A. J., Dong, X., Shi, G., and Nakajima, T.: Simulated aerosol key optical properties over global scale using an aerosol transport model coupled with a new type of dynamic core, Atmos. Environ., 82, 71–82, doi:10.1016/j.atmosenv.2013.10.018, 2014.

Diehl, T., Heil, A., Chin, M., Pan, X., Streets, D., Schultz, M., and Kinne, S.: Anthropogenic, biomass burning, and volcanic emissions of black carbon, organic carbon, and SO_2 from 1980 to 2010 for hindcast model experiments, Atmos. Chem. Phys. Discuss., 12, 24895–24954, doi:10.5194/acpd-12-24895-2012, 2012.

Dockery, D. W., Pope III, C. A., Xu, X., Spengler, J. D., Ware, J. H., Fay, M. E., Ferris, Jr., B. G., and Speizer, F. E.: An association between air pollution and mortality in six US cities, New Engl. J. Med., 329, 1753–1759, doi:10.1056/NEJM199312093292401, 1993.

Forster, P., Ramaswamy, V., Artaxo, P., Berntsen, T., Betts, R., Fahey, D. W., Haywood, J., Lean, J., Lowe, D. C., Myhre, G., Nganga, J., Prinn, R., Raga, G., Schulz, M., and Van Dorland, R.: Changes in atmospheric constituents and in radiative forcing. in: Climate Change 2007: The Physical Science Basis, Contribution of Working Group I to the Fourth Assessment Report of the Intergovernmental Panel on Climate Change, edited by: Solomon, S., Qin, D., Manning, M., Chen, Z., Marquis, M., Averyt, K. B., Tignor, M., and Miller, H. L., Cambridge University Press, Cambridge, UK and New York, NY, USA, 996 pp., 2007.

Fushimi, A., Wagai, R., Uchida, M., Hasegawa, S., Takahashi, K., Kondo, M., Hirabayashi, M., Morino, Y., Shibata, Y., Ohara, T., Kobayashi, S., and Tanabe, K.: Radiocarbon (^{14}C) diurnal variations in fine particles at sites downwind from Tokyo, Japan in summer, Environ. Sci. Technol., 45, 6784–6792, doi:10.1021/es201400p, 2011.

Goto, D., Nakajima, T., Takemura, T., and Sudo, K.: A study of uncertainties in the sulfate distribution and its radiative forcing associated with sulfur chemistry in a global aerosol model, Atmos. Chem. Phys., 11, 10889–10910, doi:10.5194/acp-11-10889-2011, 2011a.

Goto, D., Schutgens, N. A. J., Nakajima, T., and Takemura, T.: Sensitivity of aerosol to assumed optical properties over Asia using a global aerosol model and AERONET, Geophys. Res. Lett., 38, L17810, doi:10.1029/2011GL048675, 2011b.

Goto, D., Takemura, T., Nakajima, T., and Badarinath, K. V. S.: Global aerosol model-derived black carbon concentration and single scattering albedo over Indian region and its comparison with ground observations, Atmos. Environ., 45, 3277–3285, doi:10.1016/j.atmosenv.2011.03.037, 2011c.

Hasegawa, S., Kobayashi, S., Ohara, T., Tanabe, K., Hayami, H., Yomemochi, S., Umezawa, N., Iijima, A., and Kumagai, K.: Fine aerosol measurement and modeling in Kanto area (1), overview of measurement, Proceedings of the 49th Annual Meeting of the Japan Society for Atmospheric Environment, 377, 2008 (in Japanese).

Kannari, A., Tonooka, Y. Baba, T., and Murano, K.: Development of multiple-species 1 km × 1 km resolution hourly basis emissions inventory for Japan, Atmos. Environ., 41, 3428–3439, 2007.

Kinne, S., Schulz, M., Textor, C., Guibert, S., Balkanski, Y., Bauer, S. E., Berntsen, T., Berglen, T. F., Boucher, O., Chin, M., Collins, W., Dentener, F., Diehl, T., Easter, R., Feichter, J., Fillmore, D., Ghan, S., Ginoux, P., Gong, S., Grini, A., Hendricks, J., Herzog, M., Horowitz, L., Isaksen, I., Iversen, T., Kirkevåg, A., Kloster, S., Koch, D., Kristjansson, J. E., Krol, M., Lauer, A., Lamarque, J. F., Lesins, G., Liu, X., Lohmann, U., Montanaro, V., Myhre, G., Penner, J., Pitari, G., Reddy, S., Seland, O., Stier, P., Takemura, T., and Tie, X.: An AeroCom initial assessment – optical properties in aerosol component modules of global models, Atmos. Chem. Phys., 6, 1815–1834, doi:10.5194/acp-6-1815-2006, 2006.

Koch, D., Bond, T. C., Streets, D., and Unger, N.: Linking future aerosol radiative forcing to shifts in source activities, Geophys. Res. Lett., 34, L05821, doi:10.1029/2006GL028360, 2007.

Kubota, T., Shige, S., Hashizume, H., Aonashi, K., Takahashi, N., Seto, S., Hirose, M., Takayabu, Y. N., Nakagawa, K., Iwanami, K., Ushio, T., Kachi, M., and Okamoto, K.: Global precipitation map using satelliteborne microwave radiometers by the GSMaP project: production and validation, IEEE T. Geosci. Remote, 45, 2259–2275, 2007.

Kurokawa, J., Ohara, T., Morikawa, T., Hanayama, S., Janssens-Maenhout, G., Fukui, T., Kawashima, K., and Akimoto, H.: Emissions of air pollutants and greenhouse gases over Asian regions during 2000–2008: Regional Emission inventory in ASia (REAS) version 2, Atmos. Chem. Phys., 13, 11019–11058, doi:10.5194/acp-13-11019-2013, 2013.

Lamarque, J.-F., Bond, T. C., Eyring, V., Granier, C., Heil, A., Klimont, Z., Lee, D., Liousse, C., Mieville, A., Owen, B., Schultz, M. G., Shindell, D., Smith, S. J., Stehfest, E., Van Aardenne, J., Cooper, O. R., Kainuma, M., Mahowald, N., McConnell, J. R., Naik, V., Riahi, K., and van Vuuren, D. P.: Historical (1850–2000) gridded anthropogenic and biomass burning emissions of reactive gases and aerosols: methodology and application, Atmos. Chem. Phys., 10, 7017–7039, doi:10.5194/acp-10-7017-2010, 2010.

Matsui, H., Koike, M., Takegawa, N., Kondo, Y., Griffin, R. J., Miyazaki, Y., Yokouchi, Y., and Ohara, T.: Secondary organic aerosol formation in urban air: Temporal variations and possible contributions from unidentified hydrocarbons, J. Geophys. Res., 114, D04201, doi:10.1029/2008JD010164, 2009.

Mellor, G. L. and Yamada, T.: A hierarchy of turbulence closure models for planetary boundary layers, J. Atmos. Sci., 31, 1791–1806, doi:10.1175/1520-0469(1974)031<1791:AHOTCM>2.0.CO;2, 1974.

Miura, H., Satoh, M., Nasuno, T., Noda, A. T., and Oouchi, K.: A Madden-Julian Oscillation event realistically simulated by a global cloud-resolving model, Science, 318, 1763–1765, doi:10.1126/science.1148443, 2007.

Morino, Y., Chatani, S., Hayami, H., Sasaki, K., Mori, Y., Morikawa, T., Ohara, T., Hasegawa, S., and Kobayashi, S.: Evaluation of ensemble approach for O3 and $PM_{2.5}$ simulation, Asian Journal of Atmos. Environ., 4, 150–156, 2010a.

Morino, Y., Chatani, S., Hayami, H., Sasaki, K., Mori, Y., Morikawa, T., Ohara, T., Hasegawa, S., and Kobayashi, S.: Inter-comparison of chemical transport models and evaluation of model performance for O_3 and $PM_{2.5}$ prediction – case study in the Kanto Area in summer 2007, J. Jpn. Soc. Atmos. Environ., 45, 212–226, 2010b (in Japanese).

Morino, Y., Takahashi, K., Fushimi, A., Tanabe, K., Ohara, T., Hasegawa, S., Uchida, M., Takami, A., Yokouchi, Y., and Kobayashi, S.: Contrasting diurnal variations in fosil and non-fossil secondary organic aerosols in urban outflow, Japan, Environ. Sci. Technol., 44, 8581–8586, 2010c.

Moss, R. H., Edmonds, J. A., Hibbard, K. A., Manning, M. R., Rose, S. K., van Vuuren, D. P., Carter, T. R., Emori, S., Kainuma, M., Kram, T., Meehl, G. A., Mitchell, J. F. B., Nakicenovic, N., Riahi, K., Smith, S. J., Stouffer, R. J., Thomson, A. M., Weyant, J. P., and Wilbanks, T. J.: The next generation of scenarios for climate change research and assessment, Nature, 463, 747–756, doi:10.1038/nature08823, 2010.

GMDD
7, 131–179, 2014
Application of a global nonhydrostatic model
D. Goto et al.

Nakajima, T., Tsukamoto, M., Tsushima, Y., Numaguti, A., and Kimura, T.: Modeling of the radiative process in an atmospheric general circulation model, Appl. Optics, 39, 4869–4878, doi:10.1364/AO.39.004869, 2000.
Nakanishi, M. and Niino, H.: An improved Mellor–Yamada level 3 model with condensation physics: its design and verification, Bound.-Lay. Meteorol., 112, 1–31, doi:10.1023/B:BOUN.0000020164.04146.98, 2004.
Nakanishi, M. and Niino, H.: Development of an improved turbulence closure model for the atmospheric boundary layer, J. Meteorol. Soc. Jpn., 87, 895–912, doi:10.2151/jmsj.87.895, 2009.
Nasuno, T.: Forecast skill of Madden-Julian Oscillation events in a global nonhydrostatic model during the CINDY2011/DYNAMO observation period, SOLA, 9, 69–73, doi:10.2151/sola.2013-016, 2013.
Niwa, Y., Tomita, H., Satoh, M., and Imasu, R.: A three-dimensional icosahedral grid advection scheme preserving monotonicity and consistency with continuity for atmospheric tracer transport, J. Meteorol. Soc. Jpn., 89, 255–268, doi:10.2151/jmsj.2011-306, 2011.
Noda, A. T., Oouchi, K., Satoh, M., Tomita, H., Iga, S., and Tsushima, Y.: Importance of the subgrid-scale turbulent moist process of the turbulent transport: on cloud distribution in global cloud-resolving simulations, Atmos. Res., 96, 208–217, doi:10.1016/j.atmosres.2009.05.007, 2009.
Okamoto, K., Iguchi, T., Takahashi, N., Iwanami, K., and Ushio, T.: The global satellite mapping of precipitation (GSMaP) project, 25th IGARSS Proceedings, 3414–3416, 2005.
Pope III, C. A., Ezzati, M., and Dockery, D. W.: Fine-particulate air pollution and life expectancy in the United States, New Engl. J. Med., 360, 376–386, doi:10.1056/NEJMsa0805646, 2009.
Ramanathan, V., Akimoto, H., Bonasoni, P., Brauer, M., Carmichael, G., Chung, C. E., Feng, Y., Fuzzi, S., Hasnain, S. I., Iyngararasan, M., Jayaraman, A., Lawrence, M. G., Nakajima, T., Panwar, T. S., Ramana, M. V., Rupakheti, M., Weidemann, S., and Yoon, S.-C.: Atmosphere Brown Clouds and Regional Climate Change, Part I of Atmosphere Brown Clouds: Regional Assessment Report with Focus on Asia, Project Atmosphere Brown Cloud, United National Environment Programme, Nairobi, Kenya, 2008.
Randall, D. A., Heikes, R., and Ringler, T.: Global atmospheric modeling using a geodesic grid with an isentropic vertical coordinate, in: General Circulation Model Development, Academic Press, San Diego, CA, 509–538, 2000.

GMDD
7, 131–179, 2014

Application of a global nonhydrostatic model

D. Goto et al.

Sato, T., Miura, H., Satoh, M., Takayabu, Y. N., and Wang, Y.: Diurnal cycle of precipitation in the tropics simulated in a global cloud-resolving model, J. Climate, 22, 4809–4826, doi:10.1175/2009JCLI2890.1, 2009.

Satoh, M., Matsuno, T., Tomita, H., Miura, H., Nasuno, T., and Iga, S.: Nonhydrostatic Icosahedral Atmospheric Model (NICAM) for global cloud resolving simulations, J. Comput. Phys., 227, 3486–3514, doi:10.1016/j.jcp.2007.02.006, 2008.

Satoh, M., Inoue, T., and Miura, H: Evaluations of cloud properties of global and local cloud system resolving models using CALIPSO and CloudSat simulators, J. Geophys. Res., 115, D00H14, doi:10.1029/2009JD012247, 2010.

Schutgens, N., Nakata, M., and Nakajima, T.: Estimating aerosol emissions by assimilating remote sensing observations into a global transport model, Remote Sens., 4, 3528–3542, doi:10.3390/rs4113528, 2012.

Seiki, T. and Nakajima, T.: Aerosol effects of the condensation process on a convective cloud simulation, J. Atmos. Sci., online first, doi:10.1175/JAS-D-12-0195.1, 2013.

Sekiguchi, M. and Nakajima, T.: A *k*-distribution-based radiation code and its computational optimization for an atmospheric general circulation model, J. Quant. Spectrosc. Ra., 109, 2779–2793, doi:10.1016/j.jqsrt.2008.07.013, 2008.

Shimadera, H., Hayami, H., Morino, Y., Ohara, T., Chatani, S., Hasegawa, S., and Kaneyasu, N.: Analysis of summertime atmospheric transport of fine particulate matter in northeast Asia, Asia-Pac, J. Atmos. Sci., 49, 347–360, doi:10.1007/s13143-013-0033-y, 2013.

Shimizu, A., Sugimoto, N., Matsui, I., Arao, K., Uno, I., Murayama, T., Kagawa, N., Aoki, K., Uchiyama, A., and Yamazaki, A.: Continuous observations of Asian dust and other aerosols by polarization lidars in China and Japan during ACE-Asia, J. Geophys. Res., 109, D19S17, doi:10.1029/2002JD003253, 2004.

Stuhne, G. R. and Peltier, W. R.: Vortex erosion and amalgamation in a new model of large scale flow on the sphere, J. Comput. Phys., 128, 58–81, doi:10.1006/jcph.1996.0196, 1996.

Sudo, K., Takahashi, M., Kurokawa, J., and Akimoto, H.: CHASER: a global chemical model of the troposphere: 1. Model description, J. Geophys. Res., 107, 4339, doi:10.1029/2001JD001113, 2002.

Sugimoto, N., Uno, I., Nishikawa, M., Shimizu, A., Matsui, I., Dong, X., Chen, Y., Quan, H.: Record Heavy Asian Dust in Beijing in 2002: Observations and Model Analysis of Recent Events, Geophys. Res. Lett., 30, 1640, doi:10.1029/2002GL016349, 2003.

Suzuki, K., Nakajima, T., Satoh, M., Tomita, H., Takemura, T., Nakajima, T. Y., and Stephens, G. L.: Global cloud-system-resolving simulation of aerosol effect on warm clouds, Geophys. Res. Lett., 35, L19817, doi:10.1029/2008GL035449, 2008.

Takemura, T.: Distributions and climate effects of atmospheric aerosols from the preindustrial era to 2100 along Representative Concentration Pathways (RCPs) simulated using the global aerosol model SPRINTARS, Atmos. Chem. Phys., 12, 11555–11572, doi:10.5194/acp-12-11555-2012, 2012.

Takemura, T., Okamoto, H., Maruyama, Y., Numaguti, A., Higurashi, A., and Nakajima, T.: Global three-dimensional simulation of aerosol optical thickness distribution of various origins, J. Geophys. Res., 105, 17853–17873, doi:10.1029/2000JD900265, 2000.

Takemura, T., Nakajima, T., Dubovik, O., Holben, B. N., and Kinne, S.: Single scattering albedo and radiative forcing of various aerosol species with a global three-dimensional model, J. Climate, 15, 333–352, doi:10.1175/1520-0442(2002)015<0333:SSAARF>2.0.CO;2, 2002.

Takemura, T., Nozawa, T., Emori, S., Nakajima, T. Y., and Nakajima, T.: Simulation of climate response to aerosol direct and indirect effects with aerosol transport-radiation model, J. Geophys. Res., 110, D02202, doi:10.1029/2004JD005029, 2005.

Taylor, M., Tribbia, J., and Iskandarani, M.: The spectral element method for the shallow water equations on the sphere, J. Comput. Phys. 130, 92–108, doi:10.1006/jcph.1996.5554,1997.

Textor, C., Schulz, M., Guibert, S., Kinne, S., Balkanski, Y., Bauer, S., Berntsen, T., Berglen, T., Boucher, O., Chin, M., Dentener, F., Diehl, T., Easter, R., Feichter, H., Fillmore, D., Ghan, S., Ginoux, P., Gong, S., Grini, A., Hendricks, J., Horowitz, L., Huang, P., Isaksen, I., Iversen, I., Kloster, S., Koch, D., Kirkevåg, A., Kristjansson, J. E., Krol, M., Lauer, A., Lamarque, J. F., Liu, X., Montanaro, V., Myhre, G., Penner, J., Pitari, G., Reddy, S., Seland, Ø., Stier, P., Takemura, T., and Tie, X.: Analysis and quantification of the diversities of aerosol life cycles within AeroCom, Atmos. Chem. Phys., 6, 1777–1813, doi:10.5194/acp-6-1777-2006, 2006.

Tomita, H.: A stretched grid on a sphere by new grid transformation, J. Meteorol. Soc. Jpn., 86, 107–119, 2008a.

Tomita, H.: New microphysics with five and six categories with diagnostic generation of cloud ice, J. Meteorol. Soc. Jpn., 86, 121–142, 2008b.

Tomita, H. and Satoh, M.: A new dynamical framework of nonhydrostatic global model using the icosahedral grid, Fluid Dyn. Res., 34, 357–400, 2004.

Tomita, H., Miura, H., Iga, S., Nasuno, T., and Satoh, M.: A global cloud-resolving simulation: Preliminary results from an aqua planet experiment, Geophys. Res. Lett., 32, L08805, doi:10.1029/2005GL022459, 2005.

Tomita, H., K. Goto, and Satoh, M.: A new approach of atmospheric general circulation model: Global cloud resolving model NICAM and its computational performance, SIAM J. Sci. Stat. Comp., 30, 2755–2776, doi:10.1137/070692273, 2008.

Ueda, K., Nitta, H., Ono, M., and Takeuchi, A.: Estimating mortality effects of fine particulate matter in Japan: A comparison of time-series and case-crossover analysis, J. Air Water Manage. Assoc., 59, 1212–1218, doi:10.3155/1047-3289.59.10.1212, 2009.

UNEP and WMO: Integrated assessment of black carbon and tropospheric ozone, United Nations Environment Programme (UNEP) and World Meteorological Organization (WMO), Nairobi, Kenya, 2011.

Ushio, T., Kubota, T., Shige, S., Okamoto, K., Aonashi, K., Inoue, T., Takahashi, N., Iguchi, T., Kachi, M., Oki, R., Morimoto, T., and Kawasaki, Z.: A Kalman filter approach to the Global Satellite Mapping of Precipitation (GSMaP) from combined passive microwave and infrared radiometric data, J. Meteorol. Soc. Jpn., 87, 137–151, 2009.

Watanabe, M., Suzuki, T., O'ishi, R., Komuro, Y., Watanabe, S., Emori, S., Takemura, T., Chikira, M., Ogura, T., Sekiguchi, M., Takata, K., Yamazaki, D., Yokohata, T., Nozawa, T., Hasumi, H., Tatebe, H., and Kimoto, M.: Improved climate simulation by MIROC 5: Mean states, variability, and climate sensitivity, J. Climate, 23, 6312–6335, 2010.

Yu, H., Remer, L. A., Chin, M., Bian, H., Tan, Q., Yuan, T., and Zhang, Y.: Aerosols from overseas rival domestic emissions over North America, Science, 337, 566–569, doi:10.1126/science.1217576, 2012.

GMDD

7, 131–179, 2014

Application of a global nonhydrostatic model

D. Goto et al.

Table 1. Statistical values (mean of the observation and simulation, absolute bias Ba, correlation coefficient *R* and root-mean-square-error RMSE) for meteorological fields using the Stretch-NICAM-SPRINTARS simulation and observations at seven sites during the same period, as shown in Figs. 4 to 7.

	Yokohama	Chiba	Tsuchiura	Adachi	Maebashi	Machida	Kisai
	Temperature [°C]						
Observation	27.9	30.1	28.1	29.7	29.1	29.1	27.9
Simulation	26.9	28.3	28.3	27.3	25.5	25.9	25.4
Ba	−1.1	−1.8	0.2	−2.3	−3.6	−3.2	−2.6
R	0.71	0.83	0.83	0.79	0.78	0.73	0.79
RMSE	2.2	2.5	2.2	3.2	4.6	4.0	3.2
	RH [%]						
Observation	73.5	79.	73.3	75.2	73.7	75.7	71.4
Simulation	83.6	77.5	76.4	77.9	82.7	82.5	82.2
Ba	10.0	−1.5	3.0	2.8	9.0	6.8	10.7
R	0.57	0.65	0.67	0.70	0.70	0.70	0.78
RMSE	13.9	10.6	12.7	10.5	16.1	12.3	14.6
	Wind Speed [$\mathrm{m\,s^{-1}}$]						
Observation	2.9	2.6	1.6	2.6	1.2	2.7	1.9
Simulation	4.2	3.8	3.1	3.4	3.1	3.0	2.8
Ba	1.3	1.1	1.4	0.9	1.9	0.3	0.9
R	0.63	0.34	0.57	0.44	0.11	0.54	0.15
RMSE	2.1	2.3	1.9	1.9	2.5	1.6	2.0

GMDD
7, 131–179, 2014

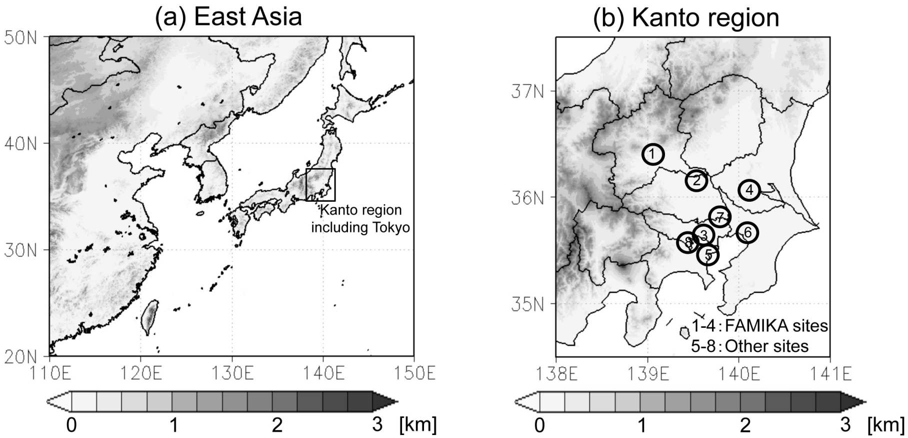

Fig. 1. Topographical maps of **(a)** Japan and **(b)** the Kanto region, including observation sites for the validation of the model. The circles represent eight sites (1. Maebashi/Gunma, 2. Kisai/Saitama, 3. Komae/Tokyo, 4. Tsukuba/Ibaraki, 5. Yokohama/Kanagawa, 6. Chiba/Chiba, 7. Adachi/Tokyo and 8. Machida/Tokyo).

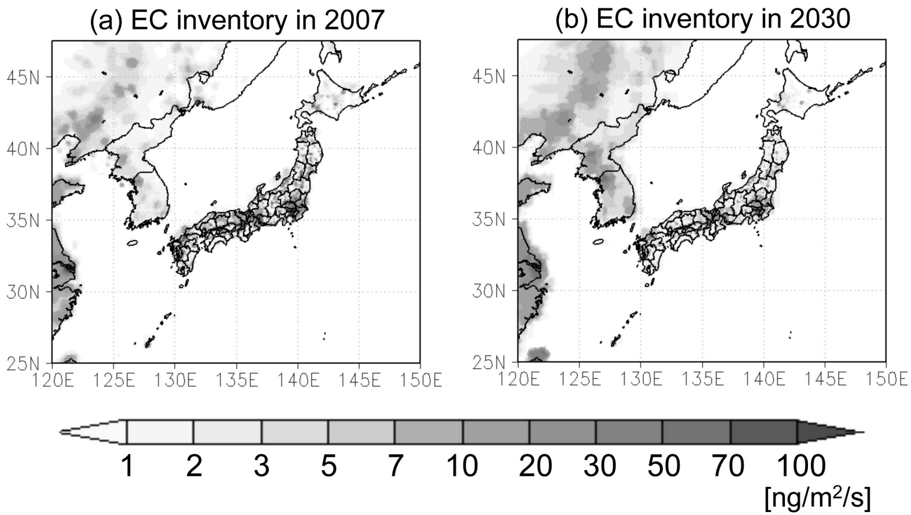

Fig. 2. EC emission inventories from **(a)** 2007 for the standard experiment and **(b)** 2030 for the RCP4.5 scenario experiment.

GMDD
7, 131–179, 2014

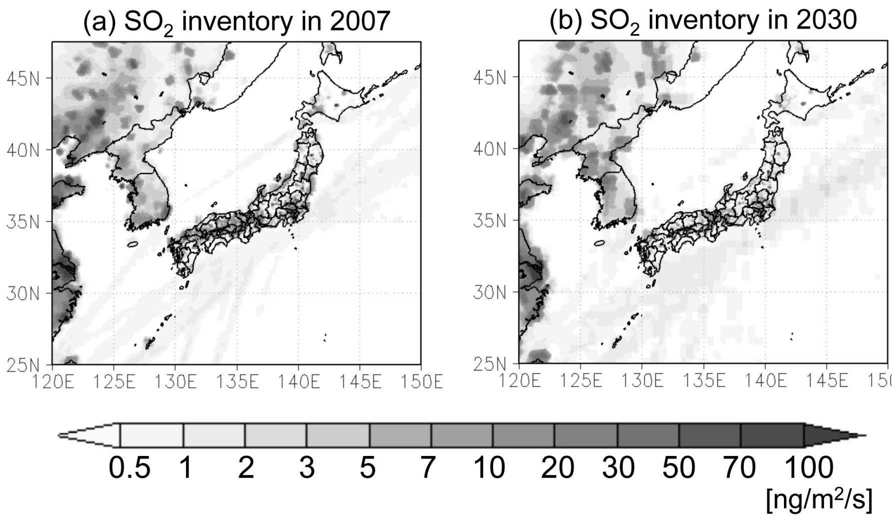

Fig. 3. Same as Fig. 2 but for SO_2 emission inventories.

GMDD
7, 131–179, 2014

Application of a global nonhydrostatic model

D. Goto et al.

Title Page
Abstract
Introduction
Conclusions
References
Tables
Figures
Back
Close
Full Screen / Esc
Printer-friendly Version
Interactive Discussion

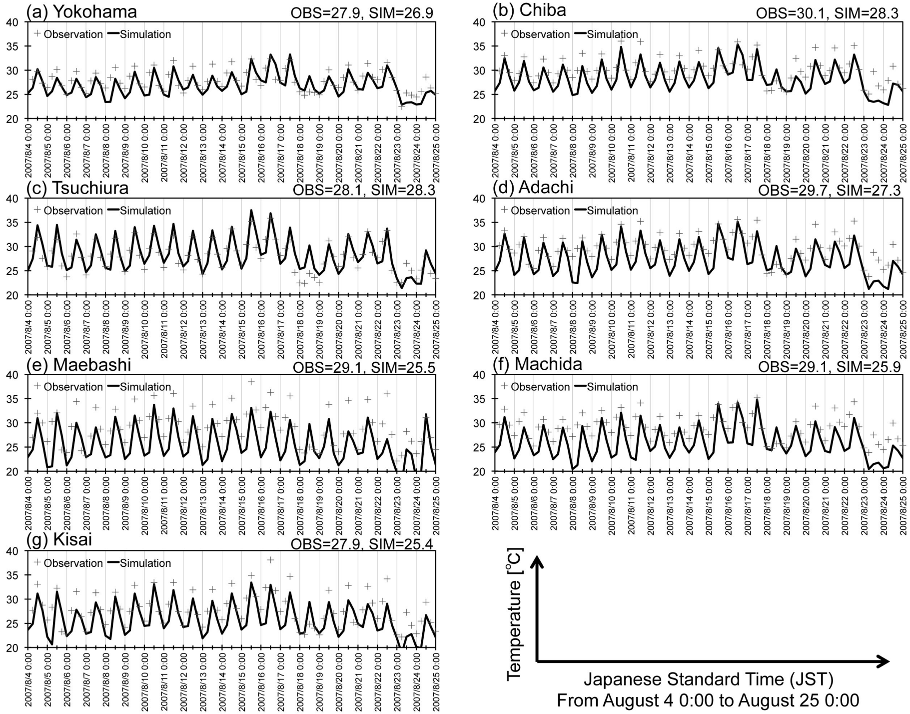

Fig. 4. Temporal variation in the Stretch-NICAM-simulated and observed air temperature for a height of 2 m at **(a)** Yokohama, **(b)** Chiba, **(c)** Tsuchiura, **(d)** Adachi, **(e)** Maebashi, **(f)** Machida and **(g)** Kisai from 4–24 August 2007. The numbers located in the upper right corner of each panel show the simulated and observed mean values.

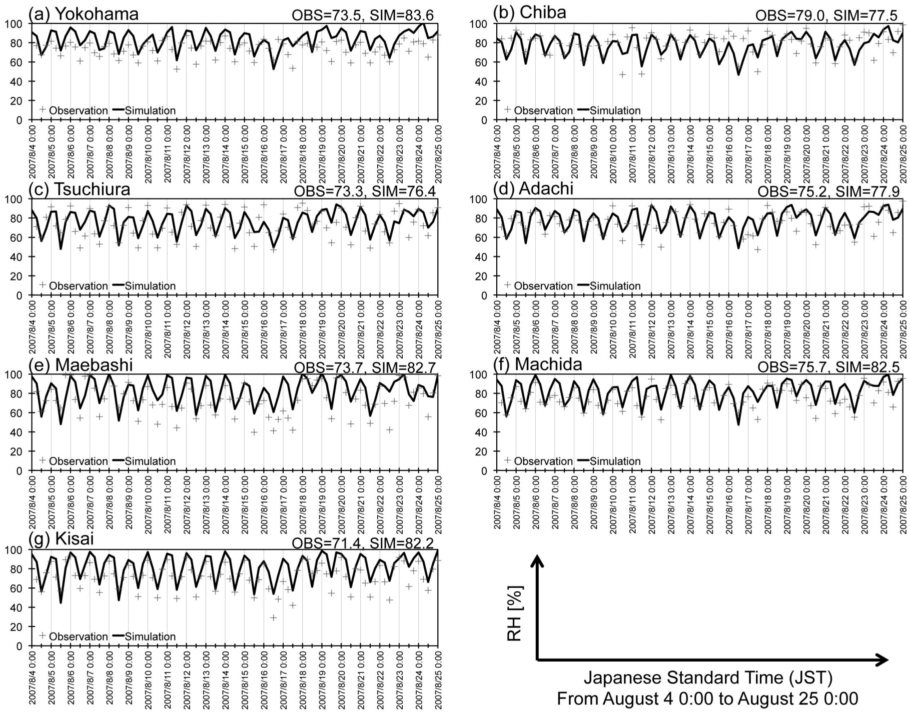

Fig. 5. Same as Fig. 4 but for relative humidity (RH).

GMDD
7, 131–179, 2014
Application of a global nonhydrostatic model
D. Goto et al.

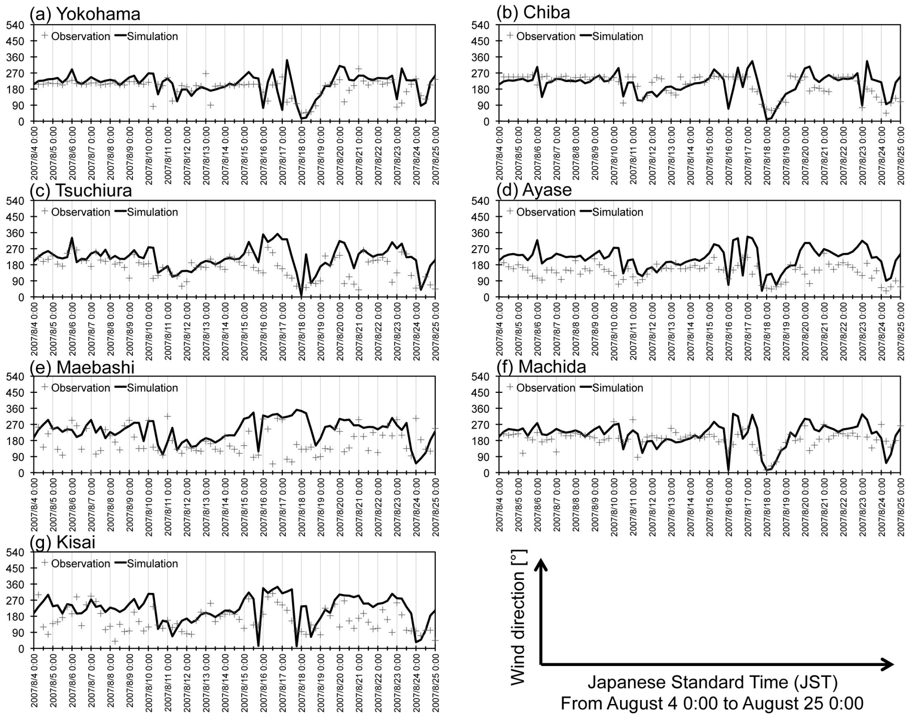

Fig. 6. Same as Fig. 4 but for wind direction.

GMDD
7, 131–179, 2014

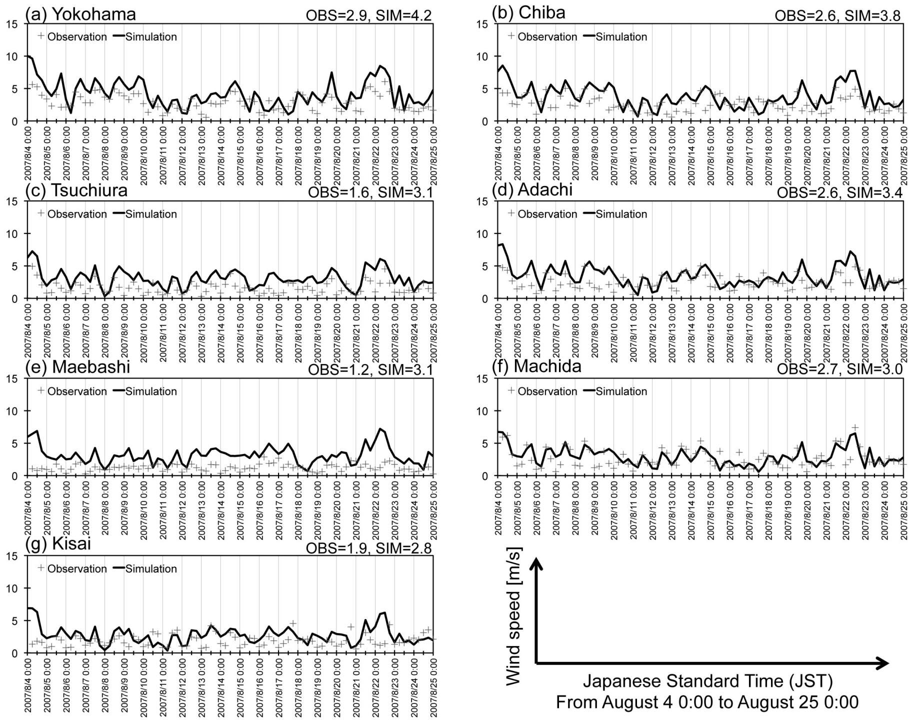

Fig. 7. Same as Fig. 4 but for wind speed.

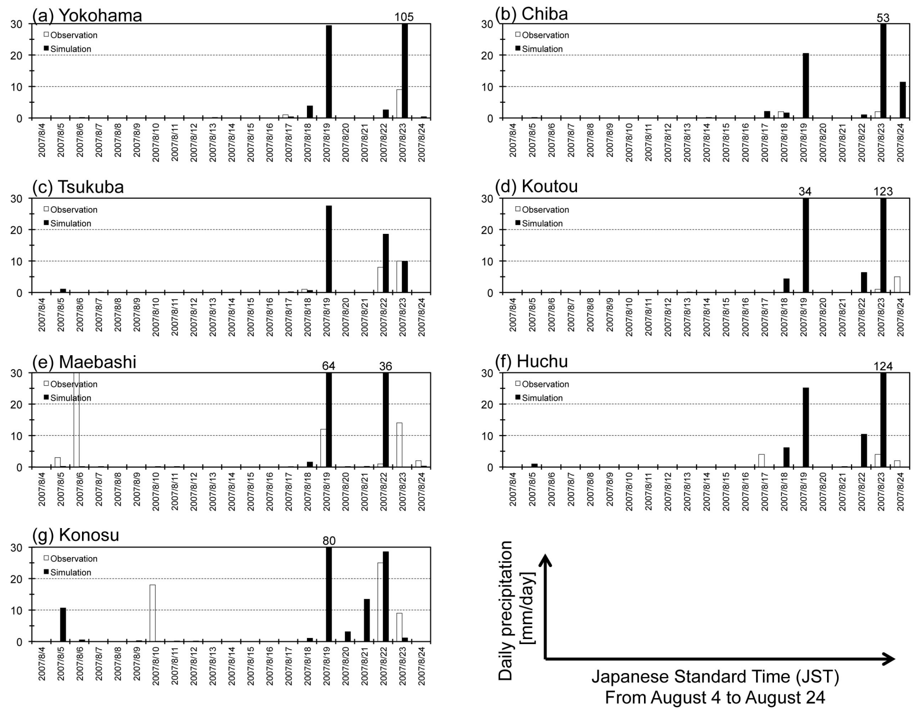

Fig. 8. Temporal variation in the simulated Stretch-NICAM-SPRINTARS and observed precipitation amounts at **(a)** Yokohama, **(b)** Chiba, **(c)** Tsukuba, **(d)** Koutou, **(e)** Maebashi, **(f)** Huchu and **(g)** Konosu from 4–24 August 2007.

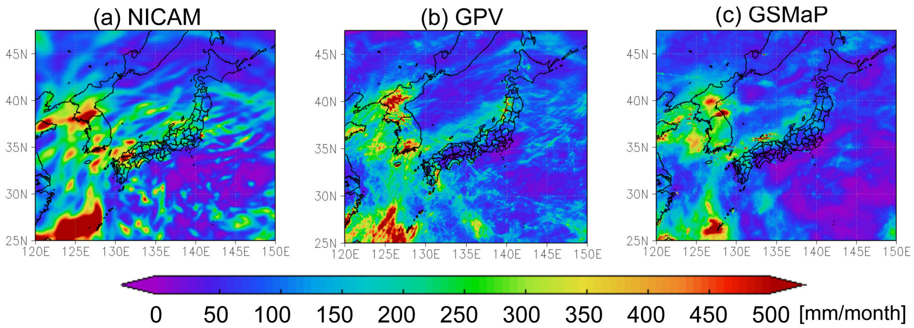

Fig. 9. Average precipitation in August derived from **(a)** Stretch-NICAM-SPRINTARS, **(b)** GPV and **(c)** GSMaP in units of mm per month.

GMDD
7, 131–179, 2014

Application of a global nonhydrostatic model

D. Goto et al.

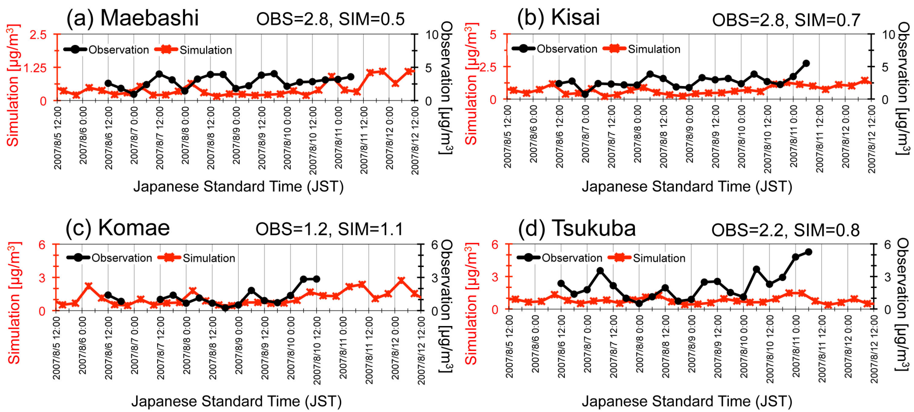

Fig. 10. Temporal variation in Stretch-NICAM-SPRINTARS-simulated and observed EC mass concentrations in units of $\mu g\,m^{-3}$ near the surface at **(a)** Maebashi, **(b)** Kisai, **(c)** Komae and **(d)** Tsukuba from 12 p.m. on 5 August 2007, to 12 p.m. on 12 August 2007. The left axis in red represents the simulated values, and the right axis in black represents the observed values.

GMDD
7, 131–179, 2014

D. Goto et al.

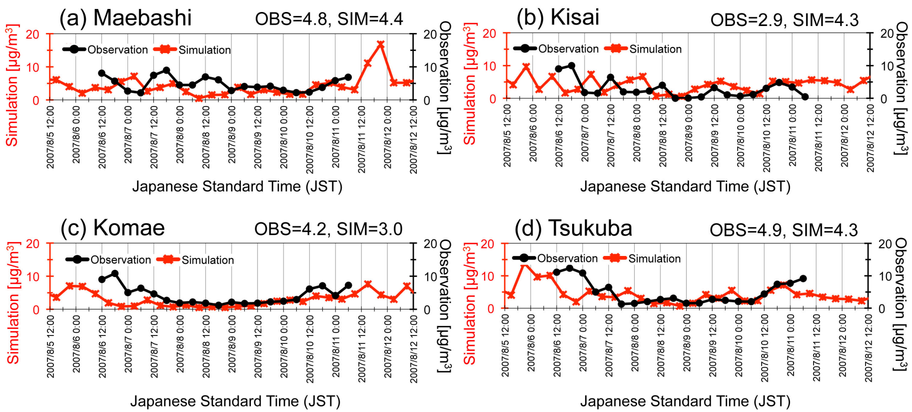

Fig. 11. Same as Fig. 10 but for sulfate.

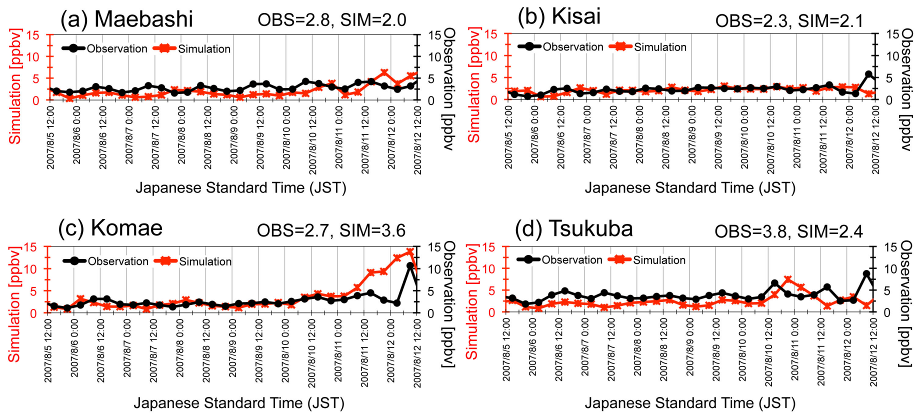

Fig. 12. Same as Fig. 10 but for SO_2, in units of ppbv.

GMDD
7, 131–179, 2014

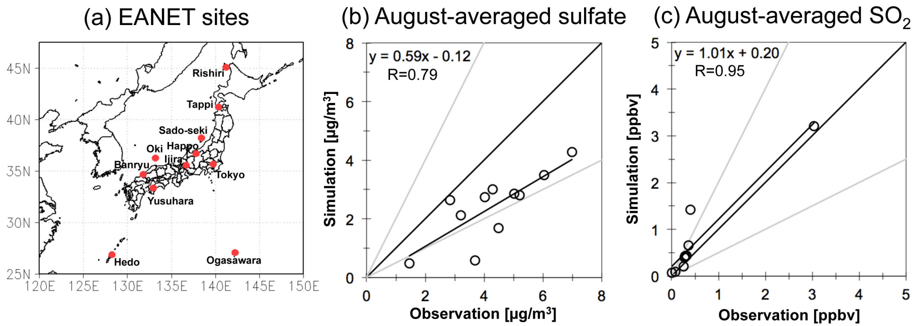

Fig. 13. Comparison of average concentrations in August for **(b)** sulfate and **(c)** SO_2 between the Stretch-NICAM-SPRINTARS simulations and the observations at EANET sites shown in panel **(a)**.

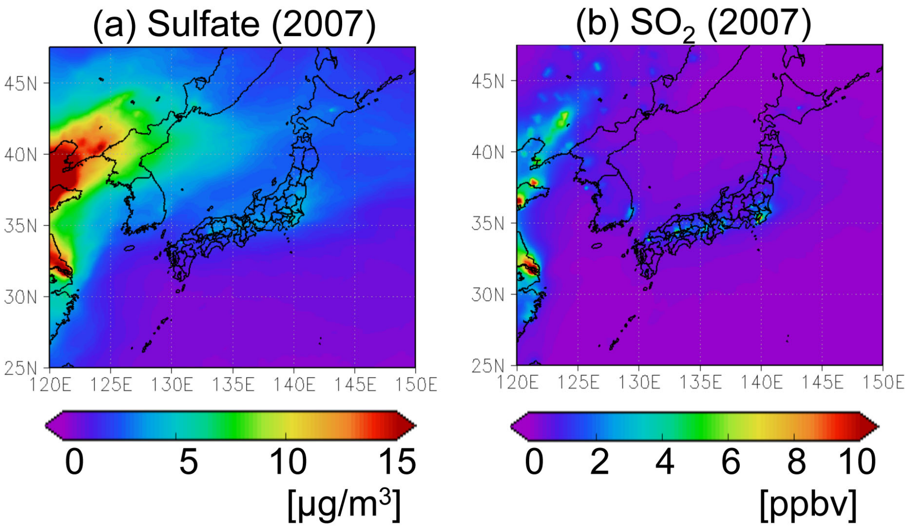

Fig. 14. Average simulated Stretch-NICAM-SPRINTARS concentrations in August for **(a)** sulfate and **(b)** SO_2 near the surface.

GMDD
7, 131–179, 2014

Application of a global nonhydrostatic model

D. Goto et al.

Title Page
Abstract Introduction
Conclusions References
Tables Figures
◀I ▶I
◀ ▶
Back Close
Full Screen / Esc
Printer-friendly Version
Interactive Discussion

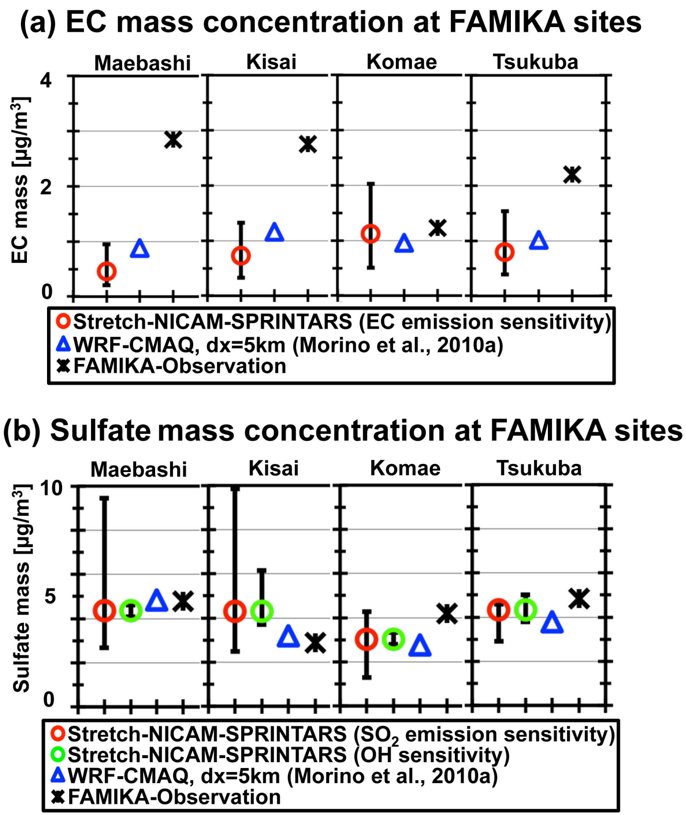

Fig. 15. (a) EC and **(b)** sulfate mass concentrations at the surface of FAMIKA sites using Stretch-NICAM-SPRINTARS results of the sensitivity experiments, WRF-CMAQ results obtained by Morino et al. (2010a) with a horizontal resolution of 5 km and the FAMIKA observation. The value and bar represent mean values from the period shown in Figs. 10 and 11.

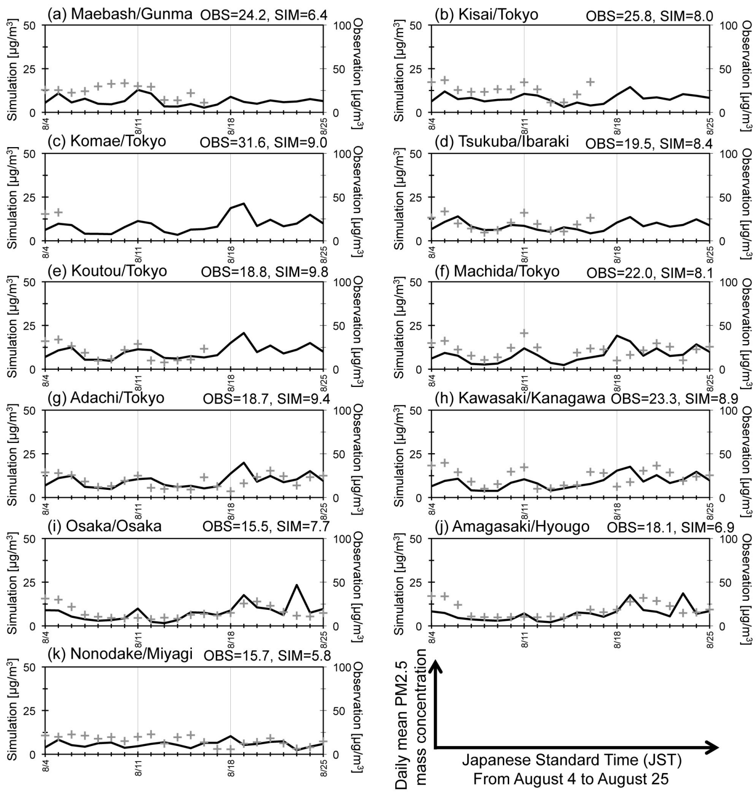

Fig. 16. Temporal variation in simulated Stretch-NICAM-SPRINTARS and observed $PM_{2.5}$ near the surface at **(a)** Maebashi, **(b)** Kisai, **(c)** Komae, **(d)** Tsukuba, **(e)** Koutou, **(f)** Machida, **(g)** Adachi, **(h)** Kawasaki, **(i)** Osaka, **(j)** Amagasaki and **(k)** Nonodake from 4–25 August 2007. The left axis in red represents the simulated values, and the right axis in black represents the observed values. The numbers located in the upper right corner of each panel show the simulated and observed mean values.

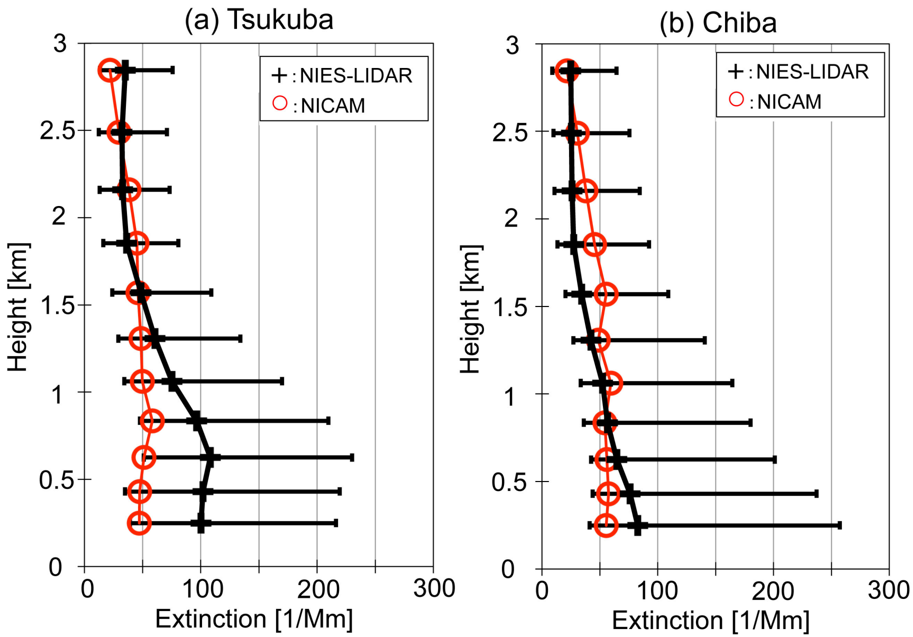

Fig. 17. Average extinction coefficients in August for the spherical particles simulated by Stretch-NICAM-SPRINTARS (shown in red) and the spherical particles observed by the NIES-LIDAR network (shown in black) at **(a)** Tsukuba and **(b)** Chiba, in units of Mm^{-1}. The bars represent the 25th and 75th percentiles of the LIDAR observations.

GMDD
7, 131–179, 2014

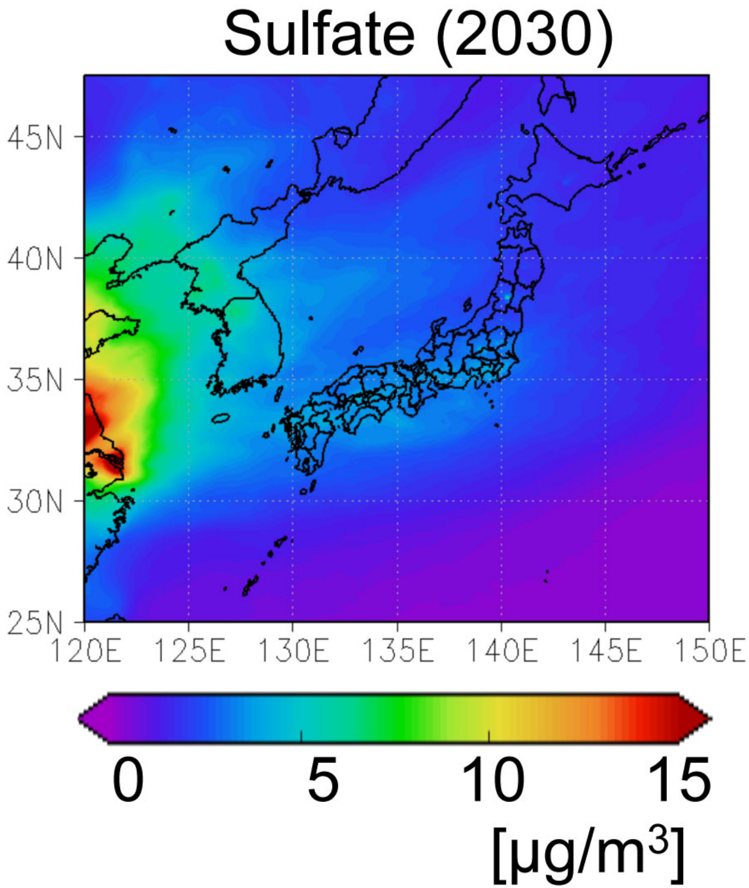

Fig. 18. Stretch-NICAM-SPRINTARS-simulated sulfate mass concentrations near the surface for August averages in the scenario experiments of RCP4.5 in 2030.

GMDD
7, 131–179, 2014

Application of a global nonhydrostatic model

D. Goto et al.

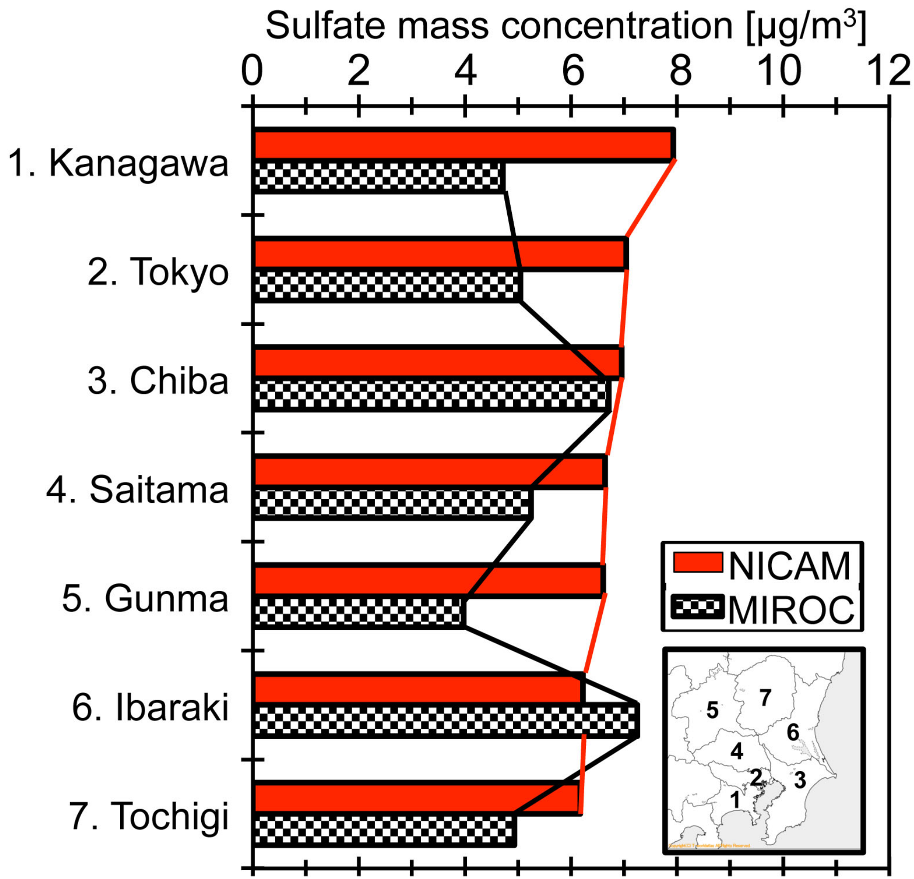

Fig. 19. Stretch-NICAM-SPRINTARS- and MIROC-AOGCM-simulated sulfate mass concentrations in each prefecture for August 2030 in the RCP4.5 scenario experiment.

GMDD
7, 131–179, 2014

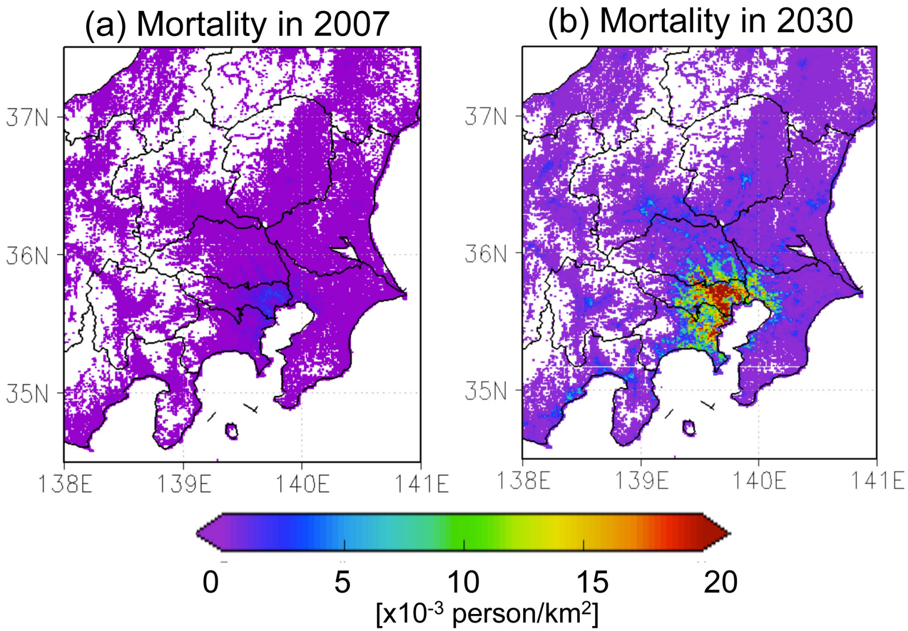

Fig. 20. Examples of the number of deaths caused by $PM_{2.5}$ in each grid of 1 km by 1 km for **(a)** the standard experiment in 2007 and **(b)** the scenario experiment of RCP4.5 in 2030 using the Stretch-NICAM-SPRINTARS simulation in the present study.

GMDD
7, 131–179, 2014